Crystallographic and magnetic properties of $R_3Fe_{29-x}V_xN_4$ (***R*** = Y, Ce, Nd, Sm, Gd, Tb, and Dy)

1998 J. Phys.: Condens. Matter 10 151

(http://iopscience.iop.org/0953-8984/10/1/017)

J. Phys.: Condens. Matter **10** (1998) 151–163. Printed in the UK PII: S0953-8984(98)82651-9

Crystallographic and magnetic properties of $R_3Fe_{29-x}V_xN_4$ (R = Y, Ce, Nd, Sm, Gd, Tb, and Dy)

Xiu-Feng Han†‡, Fu-Ming Yang†, Qian-Shu Li§, Mao-Cai Zhang‖ and Shou-Zeng Zhou‖

† State Key Laboratory for Magnetism, Institute of Physics, Chinese Academy of Sciences, PO Box 603, Beijing 100080, People's Republic of China

‡ Material Science Center, Institute of Semiconductors, Chinese Academy of Sciences, PO Box 912, Beijing 100080, People's Republic of China

§ College of Chemical Engineering and Materials Science, Beijing Institute of Technology, Beijing 100081, People's Republic of China

‖ State Key Laboratory for Advanced Materials, University of Sciences and Technology Beijing, Beijing 100083, People's Republic of China

Received 17 March 1997, in final form 8 September 1997

Abstract. A systematic investigation of crystallographic and magnetic properties of nitride $R_3Fe_{29-x}V_xN_4$ (R = Y, Ce, Nd, Sm, Gd, Tb, and Dy) has been performed. Nitrogenation leads to a relative volume expansion of about 6%. The lattice constants and unit cell volume decrease with increasing rare-earth atomic number from Nd to Dy, reflecting the lanthanide contraction. On average, the Curie temperature increases due to the nitrogenation to about 200 K compared with its parent compound. Generally speaking, nitrogenation also results in a remarkable improvement of the saturation magnetization and anisotropy fields at 4.2 K and room temperature for $R_3Fe_{29-x}V_xN_4$ compared with their parent compounds. The transition temperature indicates the spin reorientations of $R_3Fe_{29-x}V_xN_4$ for R = Nd and Sm are at around 375 and 370 K which are higher than that of $R_3Fe_{29-x}V_x$ for R = Nd and Sm 145 and 140 K, respectively. The magnetohistory effects of $R_3Fe_{29-x}V_xN_4$ (R = Ce, Nd, and Sm) are observed in low fields of 0.04 T. After nitrogenation the easy magnetization direction of $Sm_3Fe_{26.7}V_{2.3}$ is changed from an easy-cone structure to the b-axis. As a preliminary result, a maximum remanence B_r of 0.94 T, an intrinsic coercivity $\mu_0 H_C$ of 0.75 T, and a maximum energy product $(BH)_{max}$ of 108.5 kJ m^{-3} for the nitride magnet $Sm_3Fe_{26.7}V_{2.3}N_4$ are achieved by ball-milling at 293 K.

1. Introduction

The discovery of $Nd_2Fe_{14}B$ compound [1] has not only led to the appearance of the third generation of the rare-earth (R) permanent magnets, but has also stimulated many researchers to search for novel iron-rich intermetallic compounds as permanent magnet materials. Following Sm_2Fe_{17} carbides and nitrides [2] with the rhombohedral Th_2Zn_{17}-type (2:17R) structure, and $Nd(Fe, Ti)_{12}$ nitrides [3] with the $ThMn_{12}$-type (1:12) structure which show excellent intrinsic permanent magnetic properties, recently much attention has been paid to the novel intermetallic compounds $R_3(Fe, T)_{29}$ (T-transition metal) and their nitrides and carbides [4–12]. Among them, the $Sm_3(Fe, Ti)_{29}N_y$ compound [10, 11], with a strong uniaxial anisotropy and high-saturation magnetization which were very close to those of $Sm_2Fe_{17}N_{3-\delta}$, was considered as a new potential candidate for permanent magnet application.

0953-8984/98/010151+13$19.50

One can therefore believe that the nitrides and carbides of $Sm_3Fe_{29-x}T_x$ with T = V, Cr, and Mo will also have good permanent magnetic properties. For both understanding this new family and developing new hard magnet materials, a further systematic study on structure and magnetic properties of these novel 3:29 iron-rich rare-earth transition-metal intermetallic compounds is necessary. The crystallographic and magnetic properties of two series of $R_3Fe_{29-x}T_x$ (R = Y, Ce, Nd, Sm, Gd, Tb, and Dy) with T = V and Cr compounds have been studied in detail [13]. In this work, the crystallographic and magnetic properties of $R_3Fe_{29-x}V_xN_4$ (R = Y, Ce, Nd, Sm, Gd, Tb and Dy) have been investigated systematically, and the preliminary results from a study of the hard magnetic properties associated with the novel $Sm_3Fe_{29-x}V_xN_y$ magnet are reported.

2. Sample preparation and phase formation

Alloys with composition $R_3Fe_{29-x}V_x$ (R = Y, Ce, Nd, Sm, Gd, Tb, and Dy) were prepared by arc-melting the constituent elements with a purity of at least 99.9% in an argon atmosphere. The starting composition contained a 5–10% excess of rare earth relative to the stoichiometry $R_3Fe_{29-x}V_x$ to compensate the losses of the rare earths during melting and annealing. Subsequently, the ingots were annealed in sealed quartz tubes under a protective argon atmosphere at 1183–1323 K for 1–5 days in order to maximize the amount of $R_3Fe_{29-x}V_x$ phase. At the end of the annealing process, the ingots were water quenched to avoid slow cooling.

In order to prepare nitrides, the samples were pulverized into fine powder with an average particle size of about 15 μm. The nitrogenation was performed by heating the fine powder in nitrogen at an ambient pressure and at temperatures ranging from 793 to 853 K for about 2.5 h. The x-ray diffraction (XRD) patterns and thermo-magnetic analyses (TMA) show that all samples of $R_3Fe_{29-x}V_xN_y$ and their parent compounds are single phased and crystallized in the $Nd_3(Fe, Ti)_{29}$-type structure, except for an estimated amount of α-Fe in some samples.

The N concentration in the $R_3Fe_{29-x}V_xN_y$ compounds was obtained from the mass difference before and after nitrogenation. The value of y was derived to be between 4 and 4.5. Considering the excess nitrogen in the form of rare-earth nitrides under a partial decomposition of the parent compound and some α-Fe precipitation, meanwhile thinking about the slight oxidation was hard to avoid, the value of y can be taken as 4 per 3:29 formula. The obtained y value is consistent with the 3:29 structure which can be derived from alternate stacking of 2:17 and 1:12 units. The latter can hold 3 and 1 nitrogen atoms, respectively.

3. Crystallographic properties

In a unity Descartes coordinate system, the relation of the hexagonal R_2T_{17} (2:17H), tetragonal $RT_{12-x}T'_x$ (1:12), and monoclinic $R_3T_{29-x}T'_x$ (3:29) structures to the RCo_5 (1:5) structure can be given by vector transformation in reciprocal space:

$$\begin{pmatrix} h \\ k \\ l \end{pmatrix}_{2:17H} = \begin{pmatrix} -1 & -2 & 0 \\ 2 & 1 & 0 \\ 0 & 0 & 2 \end{pmatrix} \begin{pmatrix} h \\ k \\ l \end{pmatrix}_{1:5} \tag{1}$$

$$\begin{pmatrix} h \\ k \\ l \end{pmatrix}_{1:12} = \begin{pmatrix} 1 & -1 & 0 \\ 0 & 0 & 2 \\ -1 & -1 & 0 \end{pmatrix} \begin{pmatrix} h \\ k \\ l \end{pmatrix}_{1:5} \tag{2}$$

$$\begin{pmatrix} h \\ k \\ l \end{pmatrix}_{3:29} = \begin{pmatrix} -2 & -2 & 1 \\ 1 & -1 & 0 \\ 1 & 1 & 2 \end{pmatrix} \begin{pmatrix} h \\ k \\ l \end{pmatrix}_{1:5} . \tag{3}$$

The values of the determinant for the above three transformation matrices are det = 10, 6, and 4, respectively, which means that the unit cell volume of the 3:29, 2:17, and 1:12 structures is ten, six, and four times of that of the 1:5 structure, respectively. Through these transformation matrices, the relations among the 2:17H, 1:12, and 3:29 structures can be expressed in a similar way as follows

$$\begin{pmatrix} h \\ k \\ l \end{pmatrix}_{1:12} = \begin{pmatrix} 1 & 1 & 0 \\ 0 & 0 & 1 \\ \frac{1}{3} & -\frac{1}{3} & 0 \end{pmatrix} \begin{pmatrix} h \\ k \\ l \end{pmatrix}_{2:17H} \tag{4}$$

$$\begin{pmatrix} h \\ k \\ l \end{pmatrix}_{2:17H} = \begin{pmatrix} \frac{3}{5} & \frac{1}{2} & -\frac{3}{10} \\ -\frac{3}{5} & \frac{1}{2} & \frac{3}{10} \\ \frac{2}{5} & 0 & \frac{4}{5} \end{pmatrix} \begin{pmatrix} h \\ k \\ l \end{pmatrix}_{3:29} \tag{5}$$

$$\begin{pmatrix} h \\ k \\ l \end{pmatrix}_{1:12} = \begin{pmatrix} 0 & 1 & 0 \\ \frac{2}{5} & 0 & \frac{4}{5} \\ \frac{2}{5} & 0 & -\frac{1}{5} \end{pmatrix} \begin{pmatrix} h \\ k \\ l \end{pmatrix}_{3:29} . \tag{6}$$

The values of the determinant for the transformation matrices in equations (4)–(6) are det = $\frac{2}{3}$, $\frac{3}{5}$ and $\frac{2}{5}$, respectively, which also means that the unit cell volume of the 1:12 structure is two-thirds of that of the 2:17H structure, and that of the 2:17H and 1:12 structures are three-fifths and two-fifths of that of the 3:29 structure. Most Miller indices (h, k, l) found for the $R_3Fe_{29-x}T_x$ compound, except for (3, 2, 2) etc, can be identified with the corresponding ones in the R_2Fe_{17} or $RFe_{12-x}T_x$ compound. As an example, the indices (3, 3, 1), (2, 3, −1) and (2, 0, 4) of $R_3Fe_{29-x}T_x$ correspond to (3, 0, 2), (3, 0, 0) and (0, 0, 4) of R_2Fe_{17}, and the indices (2, 3, −1), (0, 4, 0) and (4, 0, −2) of $R_3Fe_{29-x}T_x$ correspond to (3, 0, 1), (4, 0, 0) and (0, 0, 2) of $RFe_{12-x}T_x$, respectively. The indices (3, 2, 2) etc, do not correspond to any indices of R_2Fe_{17} and $RFe_{12-x}T_x$, which suggests that the $R_3Fe_{29-x}T_x$ compound is not a simple mixture of the R_2Fe_{17} and $RFe_{12-x}T_x$ compounds but is a novel compound. The equivalent transformation matrices of the reciprocal vectors between the 1:5 and 2:17 (or 1:12) [14], between the 1:12 and 2:17 [15], and between 1:5 and 3:29 [8] structures were obtained, respectively, in the different coordinate systems.

The precise sites of the rare-earth atoms, Fe atoms and dumbbell Fe atoms in a unit cell of the 2:17 and 1:12 structures, corresponding to those in the unit cell of the 3:29 structure, can also be found through similar transformation matrices. This also supports the suggestion that the 3:29 structure is an ordered combination of the 2:17 and 1:12 structures in a ratio of 1:1.

As several samples, figure 1 shows XRD patterns of $R_3Fe_{29-x}V_xN_4$ (R = Ce, Gd, Tb, and Dy), collected with Cu-K_α radiation. The patterns shown in figure 1 can be quite well indexed assuming the $Nd_3(Fe, Ti)_{29}$-type structure with monoclinic symmetry and the $A_{2/m}$ space group. The easy magnetization directions (EMD) of $R_3Fe_{29-x}V_xN_4$ were deduced from the XRD patterns of the magnetically aligned powder samples, which were obtained by orienting the fine-powdered particles of $R_3Fe_{29-x}V_xN_4$ mixed with epoxy resin in a magnetic field of 1.0 T until the epoxy resin solidified at room temperature. After nitrogenation the EMD of $Sm_3Fe_{26.7}V_{2.3}$ changed from the easy-cone structure into the b-axis. Only $Sm_3Fe_{26.7}V_{2.3}N_4$ shows the uniaxial anisotropy in the series of $R_3Fe_{29-x}V_xN_4$ (R = Y, Ce, Nd, Sm, Gd, Tb, and Dy) compounds. Table 1 gives the crystallographic parameters of all parent compounds and their nitride compounds investigated here. After nitrogenation the average relative volume expansion is about 6%. It is shown that the

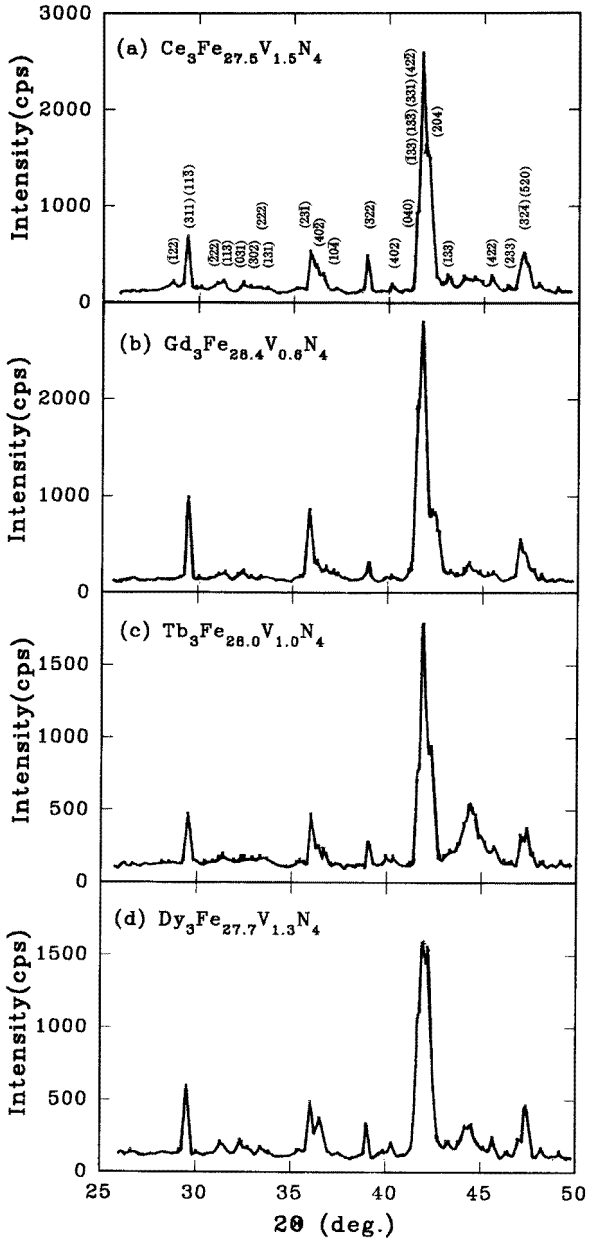

Figure 1. XRD patterns with Cu-Kα radiation observed for $R_3Fe_{29-x}V_xN_4$ (R = Ce (a), Sm (b), Gd (c) and Dy (d)).

lattice constants a, b and c and the unit-cell volume V of $R_3Fe_{29-x}V_xN_4$ and $R_3Fe_{29-x}V_x$ decreased with increasing rare-earth atomic number from Nd to Dy, except for Ce, reflecting the lanthanide contraction. The decrease of unit-cell volume leads to an increase in density with increasing rare-earth atomic number from Nd to Dy. The lattice constants a, b, and c of $Ce_3Fe_{27.5}V_{1.5}N_4$ and $Ce_3Fe_{27.5}V_{1.5}$ are unusually smaller than those of $R_3Fe_{29-x}V_xN_x$ and $R_3Fe_{29-x}V_x$ (R = Nd and Sm), respectively. This may associate with the Ce ion being

Table 1. The monoclinic lattice parameters a, b, c, β, the unit cell volume $V = abc \sin\beta$ derived based on the analysis of x-ray data with the $A_{2/m}$ space group, the x-ray density ρ derived from the lattice constraints, and the expansion $\delta V/V$ of the unit-cell volume upon nitrogenation for $R_3Fe_{29-x}V_x$ and $R_3Fe_{29-x}V_xN_4$ (R = Y, Ce, Nd, Sm, Gd, Tb, and Dy) compounds.

$R_3Fe_{29-x}V_x(N_4)$	a (Å)	b (Å)	c (Å)	β (°)	V (Å^3)	ρ (g cm^{-3})	$\delta V/V$(%)
$Y_3Fe_{27.4}V_{1.6}$	10.560	8.482	9.656	96.999	858.441	7.267	
$Ce_3Fe_{27.5}V_{1.5}$	10.553	8.495	9.675	96.717	861.396	7.837	
$Nd_3Fe_{27.0}V_{2.0}$	10.647	8.574	9.738	96.847	882.643	7.685	
$Sm_3Fe_{26.7}V_{2.3}$	10.605	8.546	9.708	96.860	873.500	7.831	
$Gd_3Fe_{28.4}V_{0.6}$	10.601	8.514	9.690	97.012	867.993	7.991	
$Tb_3Fe_{28.0}V_{1.0}$	10.565	8.482	9.665	96.903	859.811	8.079	
$Dy_3Fe_{27.7}V_{1.3}$	10.561	8.478	9.661	96.864	858.828	8.123	
$Y_3Fe_{27.4}V_{1.6}N_4$	10.719	8.654	9.862	96.528	908.949	7.068	5.9
$Ce_3Fe_{27.5}V_{1.5}N_4$	10.811	8.689	9.892	96.837	922.657	7.518	7.1
$Nd_3Fe_{27.0}V_{2.0}N_4$	10.870	8.740	9.905	97.192	933.614	7.464	5.8
$Sm_3Fe_{26.7}V_{2.3}N_4$	10.836	8.690	9.889	97.052	924.090	7.604	5.8
$Gd_3Fe_{28.4}V_{1.6}N_4$	10.796	8.672	9.849	96.931	915.360	7.781	5.5
$Tb_3Fe_{28.0}V_{1.0}N_4$	10.751	8.649	9.842	96.877	908.622	7.850	5.7
$Dy_3Fe_{27.7}V_{1.3}N_4$	10.725	8.646	9.862	96.559	908.530	7.884	5.8

non-triply ionized in each series of $R_3Fe_{29-x}V_xN_x$ and $R_3Fe_{29-x}V_x$ compounds.

Based on the expansion of the unit cell volume due to nitrogenation a good semi-empirical calculation method was used to determine the number of N atoms per unit cell of the 2:17, 1:12, and 3:29 compounds [8]. Considering the expansion $\delta V/V$ of a unit cell volume upon nitrogenation being directly proportional to the number N of nitrogen atoms in the unit cell, the ratio of the expansion in two different phases i and j can be expressed by the following equation:

$$\frac{\left(\frac{\delta V}{V}\right)_{\text{phase } i}}{\left(\frac{\delta V}{V}\right)_{\text{phase } j}} = \frac{\frac{N_{\text{phase } i}}{V_{\text{phase } i}}}{\frac{N_{\text{phase } j}}{V_{\text{phase } j}}}. \tag{7}$$

The unit cell volume ($V_{\text{phase } i}$) relation, experimental expansion $\delta V/V$ of the unit cell volume, and number of nitrogen atoms in the unit cell ($N_{\text{phase } i}$) are given in table 2. According to the relations of the unit cell volumes among the 2:17H, 2:17R, 1:12, 3:29, and 1:5 structures and the number of the N atoms in a unit cell for these phases, an average number of nitrogen atoms, about 9.12 per unit cell, is derived from equation (7). This corresponds to a N concentration of 4.56 nitrogen per 3:29 formula, which is in agreement with that obtained from the mass difference before and after nitrogenation.

4. Intrinsic and hard magnetic properties

Figure 2 shows thermomagnetic curves for the free powder samples of $R_3Fe_{29-x}V_xN_4$ (R = Y, Ce, Nd, Sm, Gd, Tb, and Dy) measured with a vibrating sample magnetometer (VSM) in the temperature range from 273 K to the Curie temperature in a low field of 0.04 T. The Curie temperature T_C of $R_3Fe_{29-x}V_xN_4$ was derived by plotting M^2 versus T curves and extrapolating M to zero. After nitrogenation the Curie temperature T_C of each nitride $R_3Fe_{29-x}V_xN_4$ increased about 200 K compared with its parent compound, except for $Ce_3Fe_{27.5}V_{1.5}N_4$ which increased about 300 K. The turning points in $M(T)$ at around 375 and 370 K correspond to the transition temperature of spin reorientations of $R_3Fe_{29-x}V_xN_4$

Table 2. The unit cell volume ($V_{\text{phase } i}$) relation, experimental expansion $\delta V/V$ of the unit cell volume, and number of nitrogen atoms in the unit cell ($N_{\text{phase } i}$) for the 2:17H, 2:17R, 1:12, and 3:29 phases. The average experimental expansion $\delta V/V$ of the unit cell volume $R_3Fe_{29-x}V_xN_y$ (R = Y, Nd, Sm, Gd, Tb, and Dy), except for R = Ce, was 5.8%. A number of about 9.12 ((8.79 + 9.21 + 9.35)/3) N atoms per unit cell was derived from equation (14).

$V_{\text{phase } i}$	$V_{3:29}/V_{\text{phase } i}$	$(\delta V/V)_{\text{phase } i}$	$N_{\text{phase } i}$	$N_{3:29}$
$V_{1:12} = 2V_{1:5}$	5/2	3.3%[a]	2	8.79
$V_{2:17H} = 6V_{1:5}$	5/3	6.3%[b]	6	9.21
$V_{2:17R} = 9V_{1:5}$	10/9	6.2%[c]	9	9.35
$V_{3:29} = 10V_{1:5}$		5.8%		

[a] From [15].
[b] From [16].
[c] From [17].

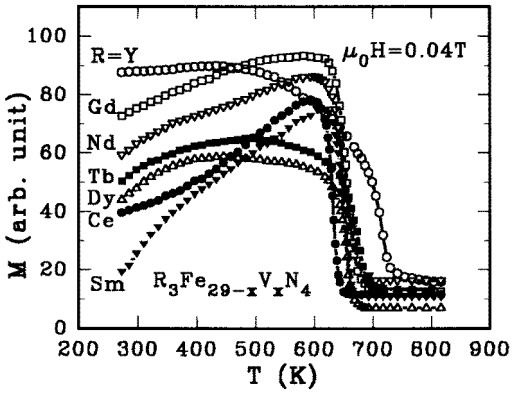

Figure 2. Thermomagnetic curves for $R_3Fe_{29-x}V_xN_4$ (R = Y, Ce, Nd, Sm, Gd, Tb, and Dy) in a low field of 0.04 T.

for R = Nd and Sm in figure 2 which increase about 145 and 140 K compared with that, at around 230 and 230 K, of their parent compounds $R_3Fe_{29-x}V_x$ for R = Nd and Sm, respectively.

It is well known that the spontaneous magnetization of the light rare-earth (R)-transition metal (T) compounds is typically decreased gradually by increasing the temperature from 1.5 K to the Curie temperature owing to the ferromagnetic coupling between the magnetic moments of the R- and T-sublattice. However, after the zero-field cooling the magnetization of $R_3Fe_{29-x}V_xN_4$ (R = Ce, Nd, and Sm), which increased gradually with increasing temperature from room temperature to about 620 K then decreased from 620 K to Curie temperature in a low field of 0.04 T, displayed an unusual behaviour as shown in figure 2. In the following field-cooling process the magnetization increased gradually with decreasing temperature from about 620 K to room temperature. As an example, figure 3 illustrates two thermomagnetic cycles for the $Sm_3Fe_{26.7}V_{2.3}$ and $Sm_3Fe_{26.7}V_{2.3}N_4$ compounds, respectively, in a low field of 0.04 T. It can be seen that after the zero-field cooling the thermomagnetic cycle from 1.5 K to room temperature and then to 1.5 K for the $Sm_3Fe_{26.7}V_{2.3}$ compound exhibits an irreversible behaviour in a low field of 0.04 T. Such effects, called magnetohistory effects [18, 19], were also observed for $R_3Fe_{29-x}T_x$ (R = Nd and Sm; T = V and Cr) [13] and $Nd_3Fe_{29-x}T_xN_4$ (T = V and Cr) [20] in a low

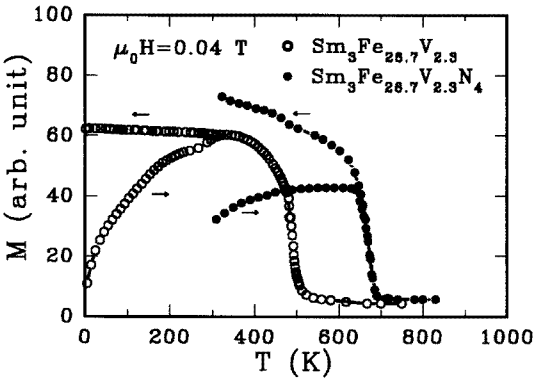

Figure 3. Thermomagnetic cycles for $Sm_3Fe_{26.7}V_{2.3}$ and $Sm_3Fe_{26.7}V_{2.3}N_4$ compounds in a low field of 0.04 T.

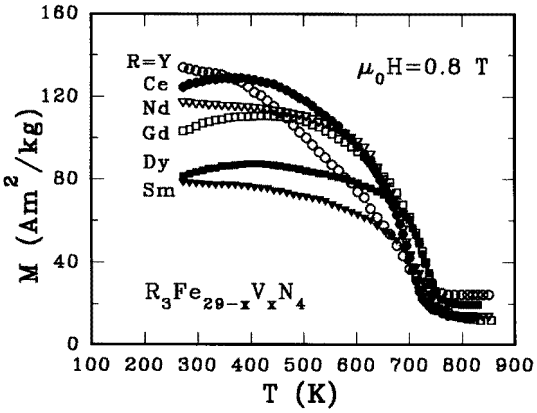

Figure 4. Thermomagnetic curves for $R_3Fe_{29-x}V_xN_4$ (R = Y, Ce, Nd, Sm, Gd, and Dy) in a field of about 0.8 T.

field of 0.04 T, it can be described based on the narrow Bloch-walls pinning mechanism [18–20]. The magnetohistory effects were not observed for $R_3Fe_{29-x}V_xN_4$ (R = Ce, Nd, and Sm) in a higher field of about 0.8 T as shown in figure 4 indicating that the domain wall pinning-field arising from the defects, such as inclusion, the second phase, etc in these compounds was smaller than 0.8 T.

For examining the amount of α-Fe impurity phases in the nitride powder samples the magnetization as a function of temperature was measured with a VSM in a field of 0.8 T on loose powder samples, which were free to be reoriented in the applied magnetic field, of $R_3Fe_{29-x}V_xN_4$ (R = Y, Ce, Nd, Sm, Gd, and Dy), and with a magnetic balance method (MBM) in a field of 1.2 T for that of $Tb_3Fe_{28.0}V_{1.0}N_4$ in the temperature range from room temperature to 900 K as shown in figures 4 and 5, respectively. It is shown that the main contribution of impurity phases to the saturation magnetization in the nitride powder samples comes from α-Fe, other impurity phases can be neglected. It is well known that the saturation magnetization value of pure iron (BCC Fe) at 4.2 K and room temperature are 221.7 A m^{-2} kg^{-1} and 217.2 A m^{-2} kg^{-1}, respectively, and the values of saturation magnetization of pure iron can be roughly thought to vary linearly in the temperature range from 4.2 K to room temperature. So the saturation magnetization contributed by the α-Fe

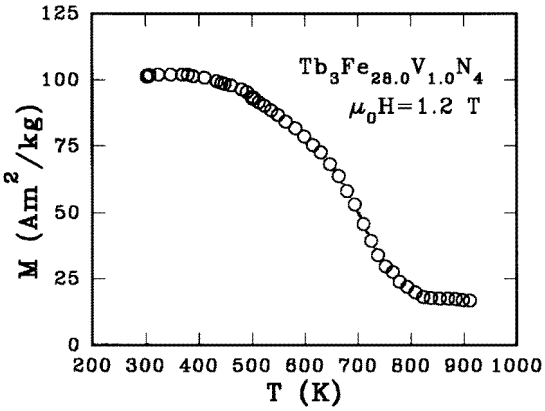

Figure 5. Thermomagnetic curves for $Tb_3Fe_{28.0}V_{1.0}N_4$ in a field of about 1.2 T.

impurity phase at room temperature and 4.2 K can be approximately derived from M versus T plots by extrapolating T from a high temperature (800– 900 K) to room temperature and then to 4.2 K as shown in figures 4 and 5. As an example, the saturation magnetization contributed by the α-Fe impurity phase to the nitride powder sample of $Tb_3Fe_{28.0}V_{1.0}N_4$ was derived to be 20.8 A m^{-2} kg^{-1} at 4.2 K and 20.4 A m^{-2} kg^{-1} at room temperature. Then the amount of α-Fe impurity phase was derived to be about 9.4 wt%, deduced from (20.4 A m^{-2} kg^{-1})/(217.2 A m^{-2} kg^{-1}).

The fine-powdered particles were mixed with epoxy resin and filled in a plastic tube of cylinder shape. A plastic tube, with the cylindrical axis parallel to the field direction for the non-spinning sample used to measure the saturation magnetization and with the cylindrical axis perpendicular to the field direction for the spinning sample used to measure the anisotropy field, was given in an applied magnetic field of about 1.0 T until the epoxy resin solidified at room temperature. The plastic tube of the spinning sample can be connected to a motor that enables the tube to be spun in an applied magnetic field. The magnetic isotherms were recorded with the external field applied either parallel or perpendicular to the alignment direction of these cylindrical samples. The magnetization curves at 4.2 K and room temperature were measured, respectively, by means of a VSM with field strength up to 7 T and pulsed magnetic fields (PMF) up to 10 T. Figure 6 shows the magnetic isotherms at 4.2 K for $R_3Fe_{29-x}V_xN_4$ (R = Y(a), Ce(b), Nd(c), Sm(d), Gd(e), Tb(f), and Dy(g)) applying the external field either parallel or perpendicular to the alignment direction of the cylindrical samples. The magnetic isotherms for $R_3Fe_{29-x}V_xN_4$ (R = Y(a), Ce(b), Nd(c), Sm(d), Gd(e), Tb(f), and Dy(g)) measured with a PMF together with the singular point detection (SPD) signal plots, dM^2/dt^2 versus H, measured by the SPD technique [21] at room temperature are given in figure 7. Singularities indicating the anisotropy field H_A at room temperature are clearly detectable from the curves of d^2M/dt^2 versus H measured on the spinning samples when H is applied parallel to the cylindrical axis, perpendicular to the aligned basal plane.

The saturation magnetization, non-deducting the contribution of the α-Fe impurity phase, at 4.2 K and at room temperature were derived from M versus $1/H^2$ plots and by extrapolating for $1/H^2$ to zero based on the high-field data of the magnetization curves measured in the external field applied parallel to the alignment direction of the cylindrical samples. The real saturation magnetization at 4.2 K and room temperature can be obtained after deducting the contribution of the α-Fe impurity phase in the samples.

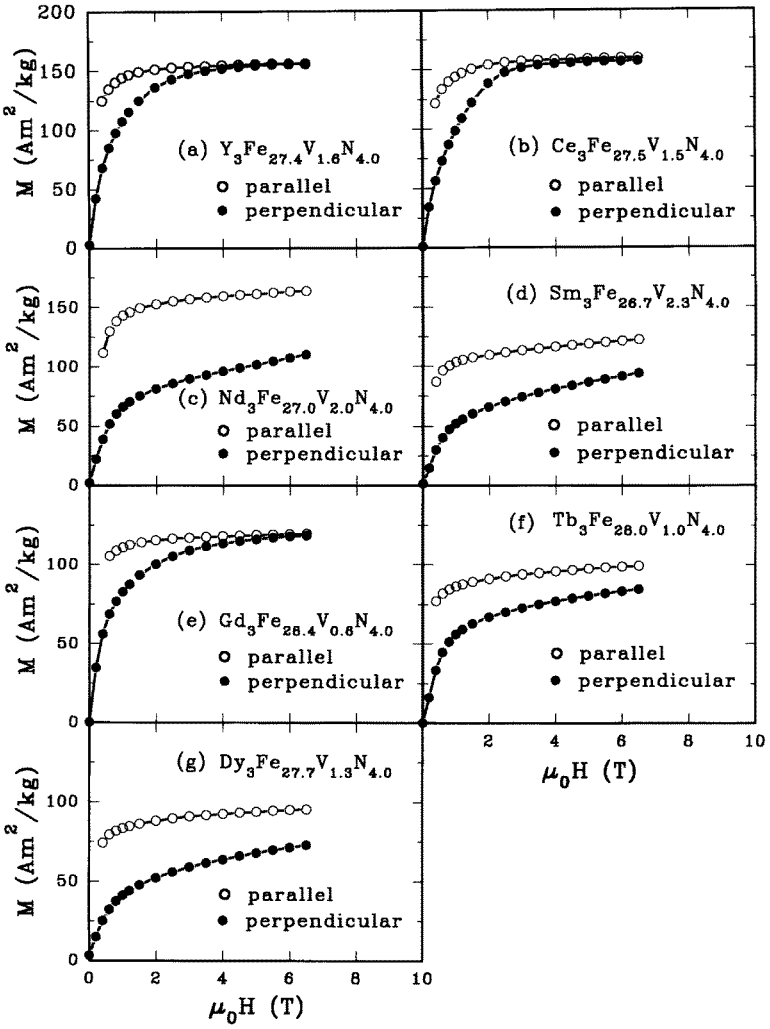

Figure 6. Isotherms at 4.2 K for $R_3Fe_{29-x}V_xN_4$ (R = Y (a), Ce (b), Nd (c), Sm (d), Gd (e), Tb (f), and Dy (g)) with the external field applied either parallel or perpendicular to the alignment direction of the powder samples.

As an example, before and after deducting the contribution of α-Fe impurity phase the saturation magnetization of $Tb_3Fe_{28.0}V_{1.0}N_4$ were 102.0 and 89.6 A m^{-2} kg^{-1} at 4.2 K and 135.7 and 127.2 A m^{-2} kg^{-1} at room temperature, respectively, which derived from (102.0–20.8) A m^{-2}/(1–0.094) kg = 89.6 A m^{-2} kg^{-1} at 4.2 K and (135.7–20.4) A m^{-2}/(1 − 0.094) kg = 127.2 A m^{-2} kg^{-1} at room temperature. The concentration y of the α-Fe impurity phase, the saturation magnetization at 4.2 K and at room temperature before and after deducting the contribution of the α-Fe impurity phase (M_S^α and M_S) in the samples are given in table 3. It was shown that correcting for the α-Fe impurity phase in the samples, which formed mainly in the process of nitrogenation due to some α-Fe precipitation under a partial decomposition of the parent compound, was necessary to obtain the values of the saturation magnetization of $R_3Fe_{29-x}V_xN_4$.

The anisotropy field H_A at 4.2 K was determined from the intersection point of

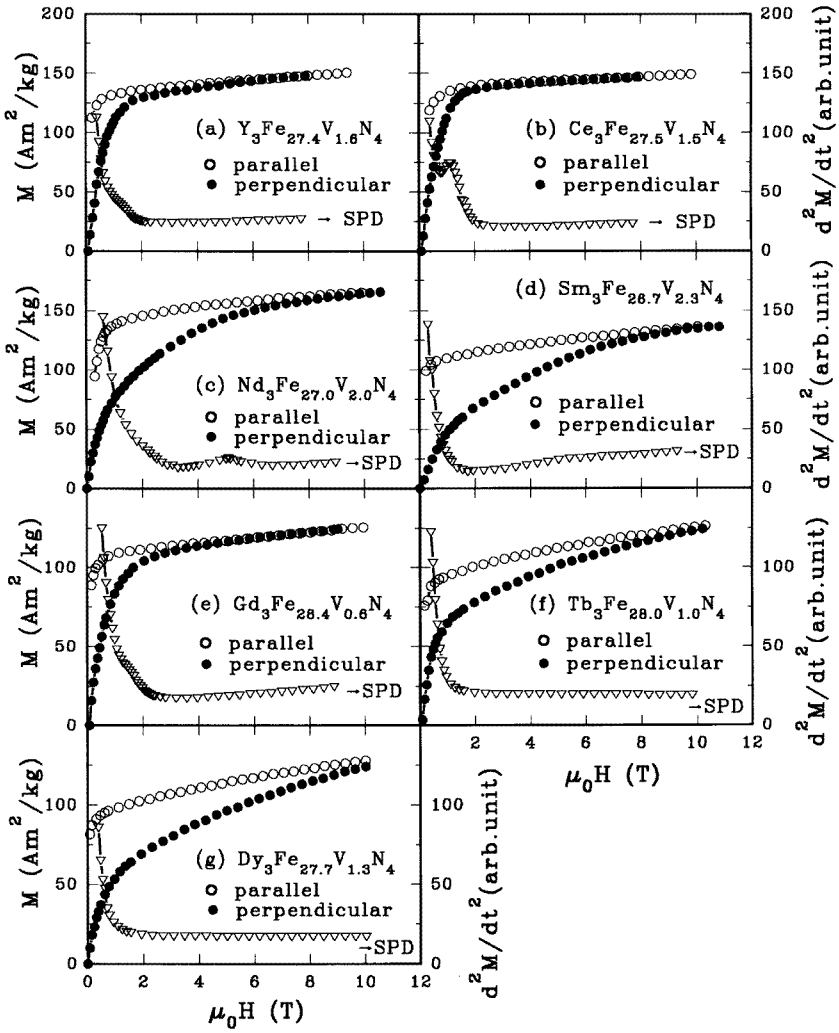

Figure 7. Isotherms and SPD signal at room temperature for $R_3Fe_{29-x}V_xN_4$ (R = Y (a), Ce (b), Nd (c), Sm (d), Gd (e), Tb (f), and Dy (g)) with the external field applied either parallel or perpendicular to the alignment direction of the powder samples.

two magnetization curves ($M_{\parallel}$–H and $M_{\perp}$–H curves), by extrapolating the linear parts, measured in the magnetic field applied parallel and perpendicular to the alignment direction of the cylinder samples. The Curie temperature, the saturation magnetization M_S and anisotropy field H_A at 4.2 K and room temperature, respectively, of these compounds of $R_3Fe_{29-x}V_xN_4$ (R = Y, Ce, Nd, Sm, Gd, Tb, and Dy) and their parent compounds are given in table 4. It can be seen that introducing N as interstitial atoms resulted generally in remarkable improvements of the Curie temperature and saturation magnetization at 4.2 K and room temperature for $R_3Fe_{29-x}V_xN_4$ compared with its parent compound. The decrease of anisotropy fields at 4.2 K and room temperature for $R_3Fe_{29-x}V_xN_4$ (R = Y, Ce, and Gd) means that the nitrogenation resulted in the decrease of the plane magnetic anisotropy for the Fe-sublattice. While the increases of anisotropy fields at 4.2 K and room temperature for $R_3Fe_{29-x}V_xN_4$ (R = Nd, Sm, Tb, and Dy) originated from the large

Table 3. The concentration y of the α-Fe impurity phase, saturation magnetization at 4.2 K and room temperature (RT) before and after deducting the contribution of α-Fe impurity phase (M_S^α) and M_S) in samples for $R_3Fe_{29-x}V_xN_4$ (R = Y, Ce, Nd, Sm, Gd, Tb, and Dy) compounds.

$R_3Fe_{29-x}V_xN_4$	y (wt%)	M_S^α (4.2 K) (A m^{-2} kg^{-1})	M_S (4.2 K) (A m^{-2} kg^{-1})	M_S^α (RT) (A m^{-2} kg^{-1})	M_S (RT) (A m^{-2} kg^{-1})
$Y_3Fe_{27.4}V_{1.6}N_4$	12.6	156.5	147.1	153.5	144.3
$Ce_3Fe_{27.5}V_{1.5}N_4$	8.4	160.5	154.9	154.4	148.7
$Nd_3Fe_{27.0}V_{2.0}N_4$	8.7	167.5	162.3	169.9	165.4
$Sm_3Fe_{26.7}V_{2.3}N_4$	9.7	128.0	117.9	143.6	135.7
$Gd_3Fe_{28.4}V_{0.6}N_4$	8.2	121.7	112.8	132.0	124.4
$Tb_3Fe_{28.0}V_{1.0}N_4$	9.4	102.0	89.6	135.7	127.2
$Dy_3Fe_{27.7}V_{1.3}N_4$	11.1	98.0	82.5	138.5	128.6

Table 4. The Curie temperature T_C, saturation magnetization M_S and anisotropy field H_A at 4.2 K and room temperature (RT) of $R_3Fe_{29-x}V_x$ and $R_3Fe_{29-x}V_xN_4$ (R = Y, Ce, Nd, Sm, Gd, Tb and Dy) compounds.

$R_3Fe_{29-x}V_x(N_4)$	T_C (K)	M_S (4.2 K) (μ_B *f.u.*$^{-1}$)	M_S (RT) (μ_B *f.u.*$^{-1}$)	μ_0H_A (4.2 K) (T)	μ_0H_A (RT) (T)
$Y_3Fe_{27.4}V_{1.6}$	435	49.6	38.6	8.3	1.7
$Ce_3Fe_{27.5}V_{1.5}$	350	50.5	32.8	5.5	1.2
$Nd_3Fe_{27.0}V_{2.0}$	455	54.7	46.8	12.8	2.4
$Sm_3Fe_{26.7}V_{2.3}$	502	42.7	33.8	8.4	4.3
$Gd_3Fe_{28.4}V_{0.6}$	518	33.6	34.7	11.2	3.6
$Tb_3Fe_{28.0}V_{1.0}$	472	25.2	26.7	13.2	4.2
$Dy_3Fe_{27.7}V_{1.3}$	449	22.7	24.7	12.8	9.4
$Y_3Fe_{27.4}V_{1.6}N_4$	633	50.9	50.0	4.0	1.2
$Ce_3Fe_{27.5}V_{1.5}N_4$	648	57.9	55.6	3.0	1.2
$Nd_3Fe_{27.0}V_{2.0}N_4$	675	61.0	62.0	17.0	5.1
$Sm_3Fe_{26.7}V_{2.3}N_4$	683	44.7	51.4	13.3	6.7
$Gd_3Fe_{28.4}V_{0.6}N_4$	678	43.3	47.8	4.6	1.5
$Tb_3Fe_{28.0}V_{1.0}N_4$	688	34.4	48.9	12.3	11.0
$Dy_3Fe_{27.7}V_{1.3}N_4$	668	31.8	49.7	14.0	11.5

increases of the uniaxial magnetic anisotropy for Sm-sublattice and the plane magnetic anisotropy for the R-sublattice (R = Nd, Tb, and Dy) after nitrogenation. The saturation magnetization of $Y_3Fe_{27.4}V_{1.6}N_4$ at 4.2 K is 50.9 μ_B f.u.$^{-1}$ which means that the average iron magnetic moment is 1.86 μ_B/Fe. The nitrogenation leads to an average iron magnetic moment increase of 0.05μ_B/Fe compared with that in $Y_3Fe_{27.4}V_{1.6}$ at 4.2 K. The transition temperature T_{sr} of the spin reorientations of $R_3Fe_{29-x}V_x$ increases from 230 to 375 K for R = Nd and from 230 to 370 K for R = Sm after nitrogenation.

The excellent intrinsic magnetic properties (T_C = 683 K, M_S(RT) = 135.7 A m^{-2} kg^{-1}, and μ_0H_A(RT) = 6.7 T) of $Sm_3Fe_{26.7}V_{2.3}N_4$ make this compound a hopeful candidate for new high-performance permanent magnets. For a $Sm_3Fe_{26.7}V_{2.3}N_4$ powder sample with an average particle size of about 10 μm, the remanence B_r of 1.03 T, intrinsic coercivity μ_0H_C of 0.52 T, and an energy product BH of 103.3 kJ m^{-3} were derived from its hysteresis loop in an external magnetic field of 7 T at 4.2 K as shown in figure 8. As a preliminary result for a nitrided $Sm_3Fe_{26.7}V_{2.3}N_4$ magnet, a maximum remanence B_r of 0.94 T, an intrinsic

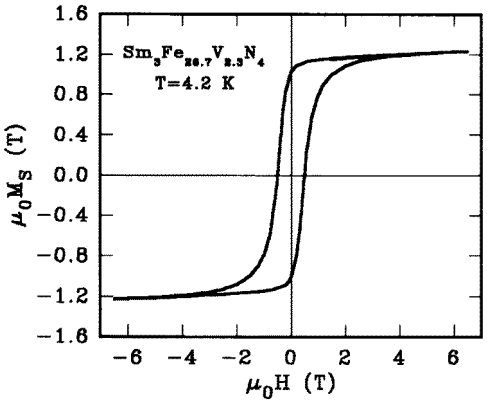

Figure 8. The hysteresis loop of $Sm_3Fe_{26.7}V_{2.3}N_4$ powder with an average particle size of about 10 μm at 4.2 K.

coercivity $\mu_0 H_C$ of 0.75 T, and a maximum energy product $(BH)_{max}$ of 108.5 kJ m^{-3} were achieved by ball-milling at 293 K.

5. Conclusions

In a Descartes coordinate system, the matrix transformation relation among the 2:17H, 1:12, 3:29, and 1:5 structures were obtained through the transformation of reciprocal vectors. This supports the suggestion that the 3:29 structure is an ordered combination of the 2:17 and 1:12 units in a ratio of 1:1. The magnetohistory effects for the $R_3Fe_{29-x}V_xN_4$ (R = Ce, Nd, and Sm) were observed in a low field of 0.04 T but were not observed in a higher field of 0.8 T showing that the domain wall pinning-field was smaller than 0.8 T. The transition temperature of the spin reorientations of $R_3Fe_{29-x}V_xN_4$ for R = Nd and Sm is at 375 and 370 K which is approximately 145 and 140 K higher than that of their parent compounds $R_3Fe_{29-x}V_x$, respectively. After nitrogenation the relative volume expansion is about 6%. The Curie temperature of each nitride $R_3Fe_{29-x}V_xN_4$ is about 200 K higher compared with its parent compound, except for $Ce_3Fe_{27.5}V_{1.5}N_4$ which increased about 300 K. Introducing N as interstitial atoms also results in remarkable improvements of the saturation magnetization and the anisotropy fields at 4.2 K and room temperature for $R_3Fe_{29-x}V_xN_4$ compared with its parent compound. After nitrogenation the EMD of $Sm_3Fe_{26.7}V_{2.3}$ changed into the b-axis from the easy-cone structure. The excellent intrinsic magnetic properties of $Sm_3Fe_{26.7}V_{2.3}N_4$ make this compound a hopeful candidate for new high-performance permanent magnets.

Acknowledgments

Project supported by the National Natural Science Foundation of China and in part by National Key Laboratory of Theoretical and Computational Chemistry, Jilin University.

References

[1] Sagawa M, Fujimura S, Togawa M and Matuura Y 1984 *J. Appl. Phys.* **55** 2083

[2] Zhong X P, Radwanski R J, de Boer F R, Jacobs T H and Buschow K H J 1990 *J. Magn. Magn. Mater.* **86** 333
[3] Yang Y C, Zhang X D, Kong L S, Pan Q and Ge S L 1990 *Proc. 11th Int. Workshop on Rare Earth Magnets and their Application* vol 2, p 190
Coey J M D and Sun H 1990 *J. Magn. Magn. Mater.* **87** L251
[4] Collocott S J, Day R K, Dunlop J B and Davis R L 1992 *Proc. 7th Int. Symp. on Magnetic Anisotropy and Coercivity in Rare Earth-Transition Metal Alloys (Canberra, 1992)* Hi-Perm Laboratory, Research Center for Advanced Mineral and Metal Procession, University of Western Australia p 437
[5] Shcherbakova Ye V, Ivanova G V, Yermolenko A S, Belozerov Ye V and Gaviko V S 1992 *J. Alloys Comp.* **182** 199
[6] Fuerst C D, Pinkerton F E and Herbst J F 1994 *J. Appl. Phys.* **76** 6144
[7] Ryan D H, Cadogan J M, Margarian A and Dunlop J B 1994 *J. Appl. Phys.* **76** 6150
[8] Kalogirou O, Psycharis V, Saettas L and Niarchos D N 1995 *J. Magn. Magn. Mater.* **146** 335
[9] Kalogirou O, Psycharis V, Gjoka M and Niarchos D N 1995 *J. Magn. Magn. Mater.* **147** L7
[10] Yang F M, Nasunjilegal B, Wang J L, Zhu J J, Qin W D, Tang N, Zhao R W, Hu B P, Wang Y Z and Li H S 1995 *J. Phys.: Condens. Matter* **7** 1679
[11] Hu B P, Liu G C, Wang Y Z, Nasunjilegal B, Zhao R W, Yang F M, Li H S and Cadogan J M 1994 *J. Phys.: Condens. Matter* **6** L197
[12] Hu B P, Liu G C, Wang Y Z, Nasunjilegal B, Tang N, Yang F M, Li H S and Cadogan J M 1994 *J. Phys.: Condens. Matter* **6** L595
[13] Han X F, Yang F M, Pan H G, Wang Y G, Wang J L, Liu H L, Tang N and Zhao R W 1997 *J. Appl. Phys.* **81** 7450
[14] Hu B P 1990 *PhD Thesis* Dublin College
[15] Psycharis V, Anagnostou M, Christides C and Niarchos D 1991 *J. Appl. Phys.* **70** 6122
[16] Sun H, Coey J M D and Hurley D P F 1990 *J. Phys. C: Solid State Phys.* **2** 6465
[17] Katter M, Wecker J, Kuhrt C and Schultz L 1992 *J. Magn. Magn. Mater.* **117** 419
[18] Barbara B, Bécle C, Lemaire R and Paccard D 1971 *J. Physique* **32** C1–299
[19] Jacobs T H, Buschow K H J, Verhoef R and de Boer F R 1990 *J. Less-Common Met.* **157** L11
[20] Han X F, Wang J L, Pan H G, Wang Y G, Liu P, Han B S and Yang F M 1997 *J. Appl. Phys.* **81** 5170
[21] Asti G and Bolzoni F 1985 *J. Appl. Phys.* **58** 1924